Kinematic Optimization of a Reconfigurable Spherical Parallel Mechanism for Robotic-Assisted Craniotomy

Terence Essomba

Department of Mechanical Engineering, National Central University 300, Jhongda Road, Jhongli City, Taoyuan County 32001, Taiwan.

Yang Hsu

Department of Mechanical Engineering, National Central University 300, Jhongda Road, Jhongli City, Taoyuan County 32001, Taiwan.

Juan Sebastian Sandoval Arevalo

Department of GMSC, Pprime Institute, CNRS - University of Poitiers SP2MI - Téléport 2 Boulevard Marie et Pierre Curie, BP 30179 86962 Futuroscope Chasseneuil Cedex, France.

Med Amine Laribi

Department of GMSC, Pprime Institute, CNRS - University of Poitiers SP2MI - Téléport 2 Boulevard Marie et Pierre Curie, BP 30179 86962 Futuroscope Chasseneuil Cedex, France.

Said Zeghloul

Department of GMSC, Pprime Institute, CNRS - University of Poitiers SP2MI - Téléport 2 Boulevard Marie et Pierre Curie, BP 30179 86962 Futuroscope Chasseneuil Cedex, France.

ABSTRACT

The craniotomy is a surgical task that is required to allow access to the patient's brain. It consists in using neurosurgical drills to open a path through the skull. The high risk resulting from Human dexterous limit justifies the use of an accurate robotic system to perform craniotomy. The present work introduces the kinematic design of a mechanism for a robotic manipulator dedicated to craniotomy. Motion capture experiments have been carried out to measure the motion of a surgical drill during the execution of craniotomy on Human cadavers. The results of the experiments are discussed. As this medical application

requires a Remote Center of Motion (RCM), a new type of 3-RRR Spherical Parallel Mechanism (SPM) is proposed to manipulate the surgical drill. The novelty of this mechanism is the integration of a reconfigurable base that re-orients the first revolute joint of the RRR legs. A mechanical architecture concept is introduced to implement this reconfiguration. It is made of three pantographic linkages that manipulate the base of the SPM. The kinematics of new mechanism is analyzed. The influence of this reconfigurable parameter is studied on two different aspects: the mechanism workspace and kinematic performances. Based on these kinematic data, the optimization of a mechanism is performed. The drill motion trajectories are used to evaluate the behavior of the optimized mechanism. It is finally compared to the classical SPM with trihedral base, showing the contribution of the new reconfiguration variable on the mechanism dexterity.

Keywords: Craniotomy, Motion capture experiments, Spherical Parallel Mechanism, Reconfigurable mechanism, Optimization, Kinematic performances.

1. INTRODUCTION

In some neurosurgery, the surgeon needs to physically access the patient's brain. However, it is protected by the skull, which is the most solid bone of Human anatomy. It is therefore required to provide an opening for the insertion of specific neurosurgical instruments. This physical access to the brain is performed by a surgical technique called craniotomy. It consists in using specific instruments to drill into the skull material [1]. There are several types of neurosurgical drills that the surgeon can use depending on the type of craniotomy to perform [2]. In full craniotomy, the entire section of the skull, namely the Bone Flap, is removed allowing a large access to the brain. The Bone Flap is usually preserved during the surgery, then re-installed on the skull for recovery. In this case, the neurosurgeon uses two types of drill. One is a semi-automatic cranial perforator

which is used to drill a series of holes radially to the skull surface [3]. These holes are made around the region to be removed. In order to preserve the patient's brain, this drill is designed to interrupt automatically when the skull reaction force is no longer detected. A second type called craniotomy cutter is then used to tangentially drill into the skull from one hole to another until the Bone Flap is completely cut off. This second instrument is combined with a dura guard, which is a hook that covers the tip of the drill to protect the brain from potential contact [4]. Also, the guard is used as reference to indicate the operator how deeply the instrument is inserted during the cutting phase. This method allows performing a craniotomy safely, even for inexperienced neurosurgeons. However, some complicated cases are not suitable with the use of these two types of surgical drill. Another type of drill, offering no automatic safety functionality but allowing higher accuracy, is then used. The tip of this drill has the shape of a ball allowing to drill both radially and axially. It is referred to as "diamond burr" or "rosen burr" depending on the surface geometry of the drill burr cut. A model of "rosen burr" type is shown on Fig. 1. Although this instrument provides more freedom of motion and flexibility, it is operated only by highly experienced neurosurgeons due to the higher level of dexterity that its manipulation requires.



Figure 1. "Rosen burr" type surgical drill for craniotomy.

Considering the high level of dexterity that is required for craniotomy in general, the use of a robotic system for the manipulation of neurosurgical drills has been continuously addressed since the end of the 1990s. Indeed, the positioning accuracy provided by robot significantly improves the quality of craniotomy. Also, the use of robotic manipulators increases the stability of the motion. Due to the effort required to drill the skull, the neurosurgeon's hand will have a brutal residual motion when the bone is completely drilled. Robotic manipulators do not suffer from such dangerous motions. For these reasons, several studies on robotic assisted craniotomy can be found in the literature. The first instance of robotic craniotomy has been reported in 1998, with the use of an industrial manipulator PUMA 260 hanging from the surgical room ceiling to perform craniofacial surgery [5]. In 2001, another robotic manipulator called "Neurobot" has been developed for craniotomy [6]. An anthropomorphic manipulator has been reprogrammed in 2003 to control the force interaction between the drill and the patient's skull in otoneurosurgery [7]. The first craniotomy trial on real patient using a robot has been perform in 2003 and reported the same year. The RobaCKa system, which is a combination between a CASPAR industrial robot and an optronic navigation system, has been used for these trials [8]. In 2006, a PA-10 industrial robot has been integrated into a tele-operated system to propose a tele-robotic skull drilling application [9]. The first nonanthropomorphic mechanical architecture used for a craniotomy robot has been reported in 2007. A Steward platform (hexapod) has been equipped with a drill mounted on an active prismatic joint. While the hexapod performs the linear and angular positioning of the drill, the device provides its longitudinal insertion [10]. The same year, an even more original architecture has been used to perform a series of simulated craniotomy on a plastic skull model. This mechanical architecture can provide the decoupled control of the drill position and orientation [11]. The "CRANIO" robotic system has been designed to perform automatic milling resection craniotomy. A series of experiments to test the accuracy of the system have been reported in 2010 [12]. A concept of Steward robot directly mounted on the patient's head to perform keyhole craniotomy has been introduced in 2012. This hexapod is reconfigurable for the maximization of its accuracy [13]. Recently, a new approach based on mechanism design has appeared in the literature. In 2016, a hybrid mechanical architecture that generates a decoupled Remote Center of Motion (RCM) has been designed [14]. A serial spherical mechanism has been optimized based on kinematic and force transmission capacity in 2015 [15]. And a parallel mechanism for spherical motion has been developed in 2018 [16].

By studying the literature review of mechanical architectures used for craniotomy procedures, it can be concluded that the two dominants tendencies are the anthropomorphic and hexapod architectures. At first, the objective of such studies was to demonstrate the feasibility of robotic assisted craniotomy, so the attention towards the architecture was limited. Later, the hexapod architecture has been selected for several prototypes due to their high accuracy. These two kind of mechanism have been used for a long period before researchers start to propose more adapted architectures. Indeed, anthropomorphic and hexapod architectures are over-dimensioned for the present application which significantly increases the acquisition price. They generate

more DoF than necessary. According to our discussions with neurosurgeons and our motion capture experiments, it appears that 2 angular DoF RCM combined with one longitudinal linear DoF is a reasonable assumption for the kinematic of this surgical task. The RCM point should be located at the center of the patient skull. However, the reported robots for craniotomy cannot generate an RCM without a complex trajectory programing, which represents a potential risk the patient. In order to manipulate the surgical drill, the use of an RCM mechanism represents a much safer and cheaper option. In the present study, the kinematic design of a robot for craniotomy is addressed by proposing a reconfigurable spherical mechanism. A preliminary kinematic analysis of this reconfigurable mechanism has been introduced in the IFToMM Symposium on Mechanism Design for Robotics in 2018 [17]. In the present extended manuscript, a more advanced kinematic analysis is provided and the mechanism concept is optimized for craniotomy application. Also, the possibility of controlling a new reconfiguration parameter to improve the kinematic behavior of the proposed mechanism is demonstrated by simulation and a feasible CAD prototype is provided. The introduction of the reconfigurable parameter allows the RSPM to perform craniotomy trajectories without significant deterioration of the dexterity. To determine the reconfigurable parameter value that optimize that mechanism dexterity, kinematic simulations are carried out. But this method is not suitable with the real time control, which will be subject to further studies. The presented mechanism is based on the kinematic data collected during a series of experiments on Human cadavers. The next Section presents the experimental protocol for the collection of these data and the results of these experiments. The third Section focuses on the kinematic analysis of a new reconfigurable Spherical Parallel Mechanism used for this application. The mechanism is then optimized to increase its kinematic performances in Section 4. In Section 5, the optimum mechanism is compared to the classical versions of the same type of mechanism. The conclusion is provided in the last Section.

2. KINEMATIC ANALYSIS OF MANUAL CRANIOTOMY

A series of medical experimentations have been carried out to collect the kinematic data associated to the practice of craniotomy. The result will allow defining the kinematic specifications of a mechanism for this application.

2.1. Experimental Protocol

The objective of the present experiments is to measure the motion of the surgical drill during a craniotomy. This measurement campaign has been carried out at the Anatomic and Biomechanics Simulation Laboratory in the Faculty of Medicine and Pharmacy of the University of Poitiers, where the access to Human cadavers has been granted. The experiments consisted in performing manual craniotomy on Human cadavers while tracking the position and orientation of the drill. The cadaver has been prepared by the neurosurgeon by removing the skin and all muscle and flesh to reveal the skull. An optronic motion capture system has been used to collect the kinematic data of the surgical drill while the surgeon was performing the craniotomy. It is typically composed of a series of synchronized cameras capable of detecting and localizing reflective markers in a 3D environment. The Qualisys motion capture (MoCap) system,

composed of a set of 8 Miqus M1 cameras with 1 MP and up to 250 fps, has been used to collect these data. In the presented study, the choice of marker sets as well as the segment reference definition were established based on the experience feedback of biomechanics research. A set of markers were fixed on the drill for position monitoring and on the expert as a visual reference. The MoCap system was then used to track and record the position of these markers. Qualisys Track Manager (QTM) software was employed to evaluate the evolution of the spatial coordinates of each marker in time, with respect to a global reference frame. The data are typically a set of coordinates for each marker as a function of time at a rate of 100Hz.

The reflective markers have been installed on the surgical drill for the measurements and several anatomical places of the cadaver's skull for reference, as show in Fig. 2. The markers attached to the frontal region of the cadaver's skull have been used to generate a reference frame that is used as a coordinate system for localizing the drill. Other markers have been placed along the longitudinal axis of the drill. Directly using the patient's anatomy as a reference is a classic method for intra-operative navigation using optronic system. The cameras have been placed around the scene. The surgical drill used for these experiment is a rosen burr type model GD-675 from Aesculap that can reach a speed or 80000 rpm. The same model is shown on Fig. 1. It is powered by electricity and activated by a ground pedal.



Figure 2. Left: Scheme of the used Qualisys motion capture system, including 8 Miqus cameras, a camera cable, a power unit, and a computer. Right: Reflective markers installed on the surgical drill and cadaver's skull.

A series of craniotomies have been performed by the neurosurgeon while the optronic system was recording. They have been done in several zones of the skull that represent an anatomical interest for the neurosurgeon, such as frontal and temporal. These zones are illustrated in Fig. 3.

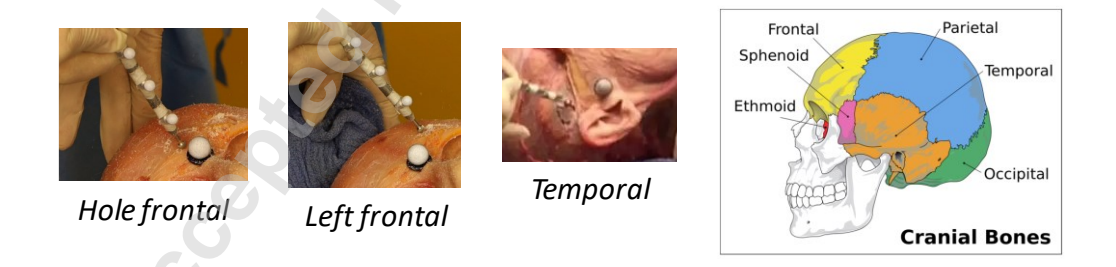


Figure 3. Anatomical zones of interest for the neurosurgeon.

2.2. Kinematic results and specification

According to the data collected from the motion capture system, the surgical drill seems to follow a specific kinematic. It appears that as the tip of the drill is following the surface of the skull, its longitudinal axis is always approximately oriented towards the center of the skull. This confirms the preliminary visual observations that led to the proposal of spherical architecture in craniotomy [14-16]. Defining the kinematic of craniotomy to a RCM which center of rotation is approximately located at the patient's skull center is a reasonable assumption that has been confirmed by the neurosurgeon involved in the experiment. According to his expertise, maintaining the longitudinal axis of the drill directed to the center of the skull allows the Bone Flap to present a trapezoidal section. This geometric characteristic will prevent the Bone Flap from falling on the patient's brain when completely cut and will facilitate its repositioning to close the skull after the surgery. Consequently, the kinematic of the surgical drill is studied in terms of angular positioning. As shown on Fig. 4, the Euler angles are chosen to describe the motion of the drill. In this study, the kinematic is limited to two angles: the drill is first rotated around its longitudinal axis, then rotated around a transversal axis, which is orthogonal to the longitudinal axis and is passing by the tip of the drill. These angles, ψ and θ , are calculated using the 3D coordinates of the markers attached to the drill. Knowing the coordinates of the drill longitudinal axis allows determining the two Euler angles mentioned above.

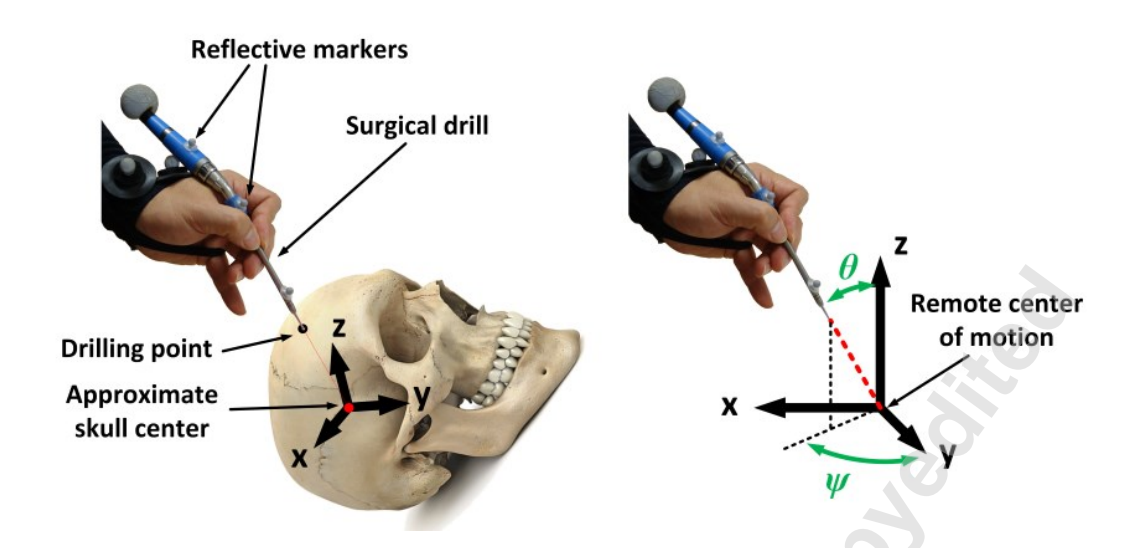


Figure 4. Kinematic of the surgical drill in craniotomy.

For each region of the cadaver's skull, the reference frame was constructed to orient its \mathbf{z} axis approximatively normal to the skull surface. Based on this coordinate system, the orientation angles of the drill was recorded during several craniotomy operation. The evolution of these angles are displayed in Fig. 5. The computed angle boundaries for the four locations, shown on Fig. 3, are given in Table 1, which represent the most explored locations in craniotomy. One observe that value of angle θ does not go greater than 14°.

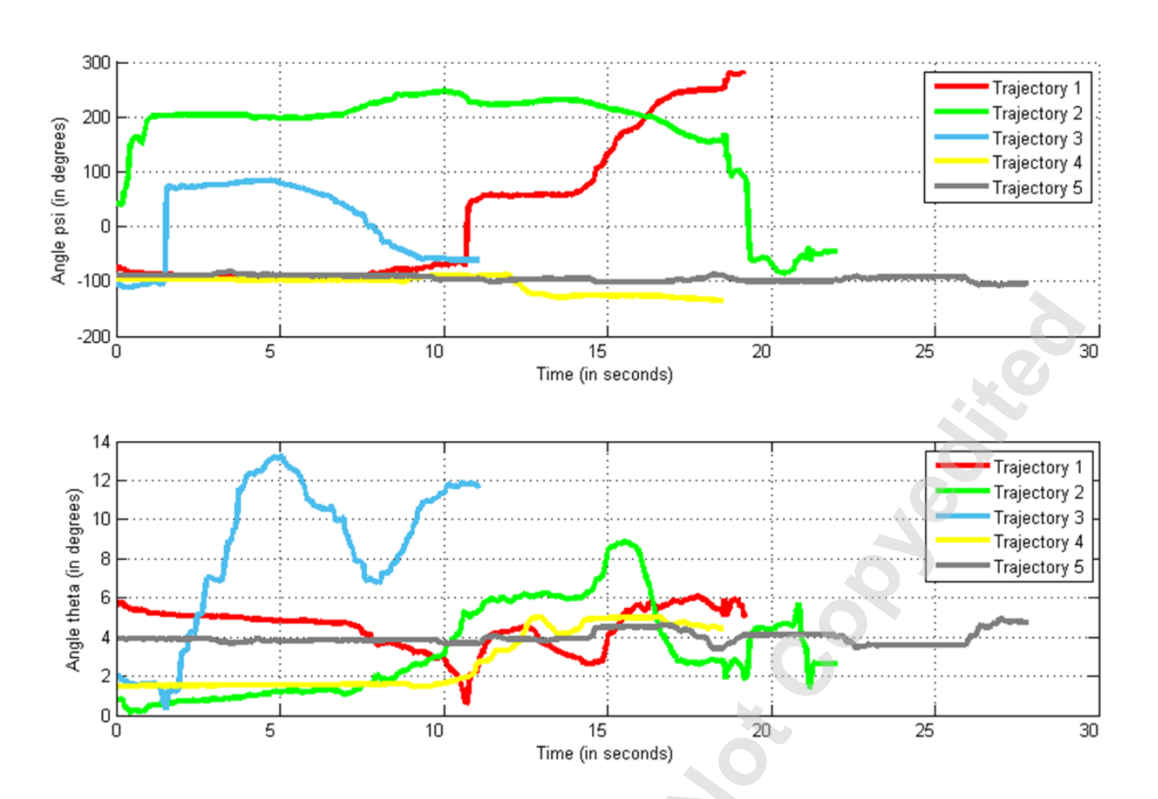


Fig. 5. Evolution of the drill orientation angles during the craniotomy operation on Human cadaver.

Table 1. Bounding values for orientation angles.

		Locations							
Angles (°)		Hole frontal Trajectory 1	Left Frontal Trajectory 2	Right Frontal Trajectory 3	Left Temporal Trajectory 4	Right Temporal Trajectory 5			
ψ	Min	-94.6	-85.7	-111.3	-134.6	-108.5			
	Max	283.7	247.6	84	-88.4	-81.1			
θ	Min	0.6	0.2	0.3	1.4	3.4			
	Max	6.1	8.9	13.3	5	4.6			

3. SPHERICAL PARALLEL MECHANISM WITH RECONFIGURABLE BASE

A specific mechanical architecture is proposed for this neurosurgical application.

The kinematic effects of the architectural modifications on this mechanism are studied in this Section.

3.1. Mechanical Architecture Definition and Kinematic Model

Based on the results of the previous Section, a series of kinematic requirement have been established. According to the recent literature review on craniotomy robot, RCM mechanical architectures seem to be more adapted. Therefore, the use of Spherical Parallel Mechanism (SPM) is proposed for this application. The SPM is known for displacing its end-effector on paths located on a spherical surface of a given radius. This particular kinematics is called Remote Center of Motion (RCM). In other words, the endeffector can rotate around any axis passing through a fixed point, which is the center of the sphere. To manipulate their end effector with 3 angular Degrees of Freedom (DoF), some SPM are composed of three legs connecting a moving platform (end-effector) to a fixed base. Different approaches deal with SPM in literature. Designs based on 3-RRR legs were introduced in [18] and the Agile Eye in [19] Material and dimensional optimization for a 3-CRU type is presented in [20]. The required torques to ensure a correct trajectory and speed for a 3-RRP is studied in [21]. And the suppression of internal unnecessary mobilities for a 3-RUU is described in [22,23]. The design of SPM focuses on the size of its orientation workspace as well as kinematics performances, as for 3-RRR structure [24,25]. The obtained optimal solution is often linked to specific requirements. In order to cope with this limitation, reconfigurable solutions could be investigated. The advantages of developing re-configurable systems include adaptability, reusability, convertibility,

compactness, fault-tolerance and emergency behavior [26]. A configuration concept is introduced in to change robot characteristics in operation in [27]. The classical 3-RRR planar mechanism has been compared to a 4-RRR reconfigurable version that presents one additional leg. The second mechanism showed higher kinematic and dynamic performances [28]. A 9-DoF 3-PPPRS reconfigurable mechanism has been compared with three other non-reconfigurable 6-DoF mechanisms (3-PRPS, 3-PPRS and 3-PRRS) and has shown superior static and dynamic stiffness [29]. A parallel mechanism made of three reconfigurable rTPS legs has been presented with a unified kinematic model. The first Hooke (rT) joint of each legs allows two different working phases [30]. Recently, a 3-PRPR parallel mechanism with reconfigurable base has been reported. By adjusting the geometric configuration of the base, the mechanism shows improved workspace, stiffness and dexterity [31]. A 4-RRS mechanism with a reconfigurable parallelogram linkage mobile platform has been studied in terms of transferability [32].

The main approaches that have been proposed for reconfiguration of parallel mechanisms are aimed to adapt them to the environment and task changes. Such a method has been proposed to increase the accuracy of the robot during the craniotomy [33]. In the present study, the geometric reconfiguration of a 3-RRR SPM base is provided by the mean of pantographic linkages. The motion given by these pantographic linkage generate a new reconfigurable parameter, which effect on the workspace and the dexterity is investigated. The original SPM is made of three serial spherical arms that connect the base to the end effector. Each of them is composed of two spherical linkages which dimensions are respectively measured by the angle α between z_{1k} and z_{2k} and δ

between z_{2k} and z_{3k} . The input variables of the mechanism are given by the angles measured at the first revolute joint of each arm. All other joints are passive. The platform of this mechanism is located by the axis z_E that passes through its center. Its dimension is measured by the angle γ between z_{3k} and z_E . Classically, the active revolute joint axes of the SPM are disposed as a trihedral form. Which means that z_{1A} , z_{1B} and z_{1C} are oriented as the three orthogonal axes x, y and z of a reference frame.

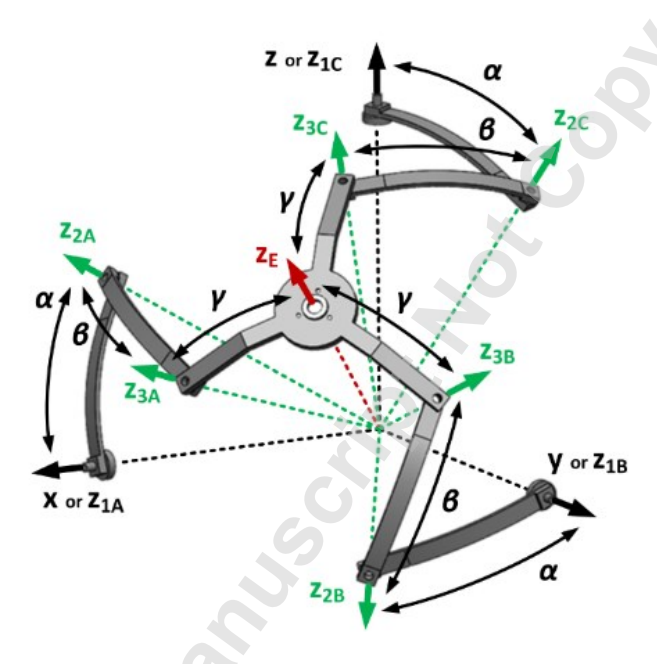


Figure 6. Kinematic drawing of the 3-RRR Spherical Parallel Mechanism.

A new design parameter is introduced for the geometric reconfiguration of the SPM base. A similar concept has been presented in order to identify an optimum 3-RRR SPM for tele-echography [25]. However, although this new parameter was introduced as an additional design variable, its effect on the mechanism characteristics such as workspace size or kinematic performances was not investigated. The main weakness of the classical 3-RRR SPM is the instability of its kinematic behavior over its workspace, which is excellent at the workspace center but rapidly deteriorates when moving away

from it. One of the contribution of this study is to improve that behavior by introducing a reconfigurable parameter. As a mechanical architecture made of three serial spherical arms, it is mandatory that all revolute joint axes are directed to the center of rotation, including the input joints $\mathbf{z_{1A}}$, $\mathbf{z_{1B}}$ and $\mathbf{z_{1C}}$, which constitute the mechanism base. The center of the workspace is represented by the axis $\mathbf{z_{W}}$. It is located at the same fixed angle λ from each reference frame axes \mathbf{x} , \mathbf{y} and \mathbf{z} . In the present proposal, the base of each RRR arm $\mathbf{z_{1k}}$ is oriented by an angle ω from the one reference frame axis respectively. This angle ω is formed on the planes (Oxz_W) , (Oyz_W) and (Ozz_W) as shown in Fig. 7. The calculation of the angle λ is explained bellow.

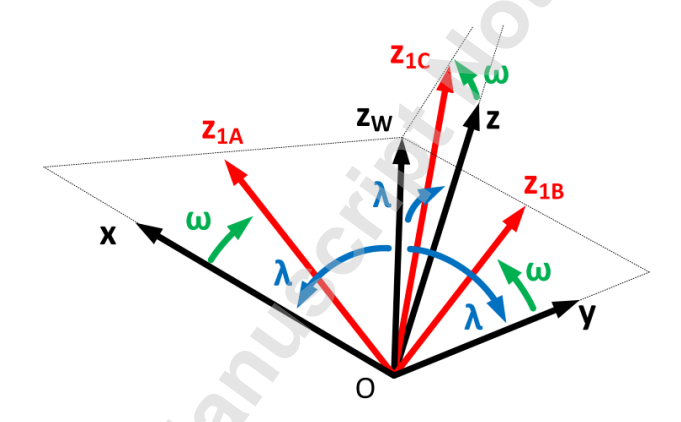


Figure 7. Kinematic of the base SPM reconfigurable base.

To obtain a technically feasible mechanism, it is proposed to orient the mechanism joints axes z_{1A} , z_{1B} and z_{1C} using a pantographic linkage of each of them, as illustrated in Fig. 8. It should be noted that the mechanism shown on this CAD model is destined to serve as a prototype for preliminary testing. In a final version, it is planned to mount the pantograph linkage above the SPM mechanism. This architecture is known to generate a RCM of one DoF. The base of each pantographic linkage is attached to a common central base while their output linkage is attached to one RRR arm of the SPM. Their positions

have been specifically adjusted so that their center of rotation corresponds to the 3-RRR SPM center of rotation. All pantographic mechanisms generate the same rotation at the same time. This synchronization is provided by two transmission stages. The first one consists in a central gear that transfers the revolute motion of a motor to three satellite gears. In the second stage, each satellite gear is attached to a worm gear combination that guide the rotation of the input joint of one pantographic mechanism. The motor can then control the configuration of all the pantographic mechanisms at once by rotating their horizontal linkage. Particularly, the angular position of the upper horizontal linkages that are attached to the SPM base (z_{1k}) , will rotate around the whole mechanism center of rotation. Therefore, the synchronized control of the three pantographic linkages will re-orient the SPM active revolute joint axes z_{1A}, z_{1B} and z_{1C} around the same center of rotation around the axes \mathbf{x}_{ω} , \mathbf{y}_{ω} and \mathbf{z}_{ω} respectively, as presented in Fig. 6. The classical base configuration can be obtained by setting ω to 0. In this configuration, the mechanism base represented by axes z_{1A}, z_{1B} and z_{1C} will form a trihedral shape and axes mentioned will be confused with axes x, y and z respectively. From this position, increasing ω in the positive direction ($\omega > 0$) will reduce the size of the mechanism base as the first revolute joints of each RRR arm is moving toward the workspace center, meaning that axes z_{1k} are rotating toward the axis zw. This reconfiguration is literally referred to as "closing the base". On the other hand, "opening the base" can be carried out by increasing the angle ω in the negative direction, which will re-orient the z_{1k} axes away from the workspace center.

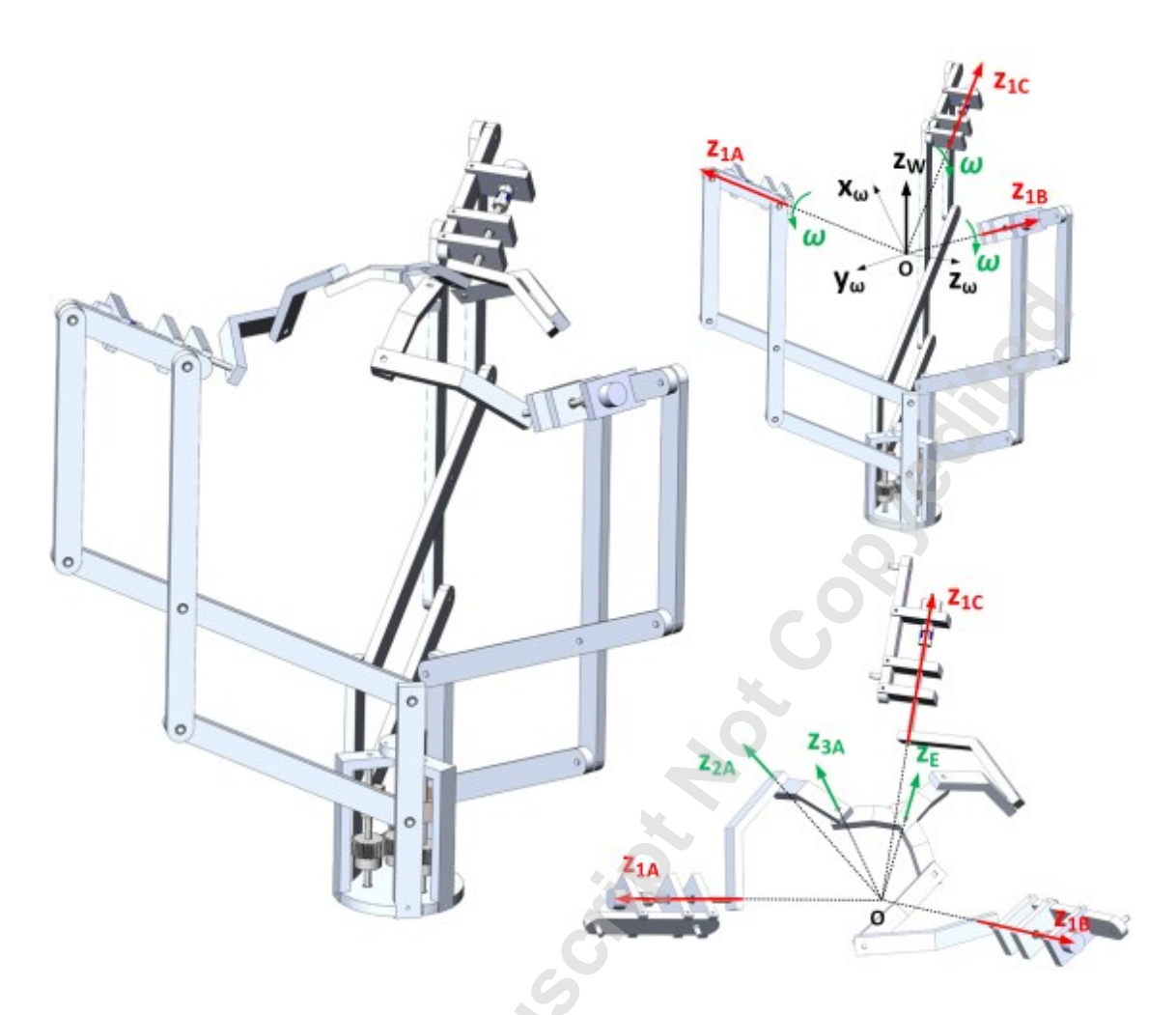


Figure 8. Conceptual CAD of the 3-RRR Reconfigurable Spherical Parallel Mechanism.

By its particular architecture, the 3-RRR SPM generates a Remote Center of Motion (RCM). In order to simplify the present study, the radius of the resulting spherical motion is assumed to be equal to one. Here, the mobile platform is located by 3 Euler angles. The origin position is represented by an axis, namely $\mathbf{z}_{\mathbf{w}}$ of coordinates $[1/\sqrt{3} \ 1/\sqrt{3} \ 1/\sqrt{3}]$, which is located at the middle between the \mathbf{x} , \mathbf{y} and \mathbf{z} unit vectors of a reference frame. From this origin, the end effector is moved by the angle ψ , θ and φ . The rotation matrix $\mathbf{R}_{\mathbf{E}}$ associated with the end effector in this particular location can therefore be calculated by the successive rotations bellow:

$$\mathbf{R}_{\mathbf{E}} = \mathbf{R}_{\mathbf{z}}(\pi/4) \cdot \mathbf{R}_{\mathbf{v}}(\lambda) \cdot \mathbf{R}_{\mathbf{z}}(\psi) \cdot \mathbf{R}_{\mathbf{x}}(\theta) \cdot \mathbf{R}_{\mathbf{z}}(\varphi), \tag{1}$$

With $\mathbf{R}_{\mathbf{u}}(\alpha)$, rotation matrix of angle α , about axis \mathbf{u} . The two first rotation matrices allow centering the end effector on the axis $\mathbf{z}_{\mathbf{W}}$. In this regards, it is necessary to rotate $\pi/4$ around the \mathbf{z} axis to place the \mathbf{y} axis normal to the plane (Ozzw). The angle λ has been calculated to be around 54.74 degrees or 0.955 radian. The rotation matrix \mathbf{R}_{E} can be also interpreted as the reference frame attached to the manipulator end effector.

The inverse kinematic model (IKM) of the 3-RRR SPM has been already addressed in [25]. The resolution method consists in finding, for each RRR leg, the input coordinate θ_{1k} that places the second joint \mathbf{z}_{2k} at an angle of $\boldsymbol{\theta}$ from the third joint \mathbf{z}_{3k} which is located by the end effector. This can be described as followed:

$$\mathbf{z}_{2k} \cdot \mathbf{z}_{3k} = \cos \beta, \tag{2}$$

With k = A, B or C, referring to the mechanism RRR legs.

The IKM of the 3-RRR SPM can be resolved by finding the solution of Eq. (2). For each arm, the coordinates of the joint axes \mathbf{z}_{3k} are calculated using the rotation matrix \mathbf{R}_{E} and additional ones that include the angle γ . The axis \mathbf{z}_{2k} is calculated by the angle α , the input coordinate θ_{1k} and the angle ω that gives the orientation of the base located by \mathbf{z}_{1k} . The SPM base axes coordinates are now obtained as follows:

$$\begin{cases}
\mathbf{z}_{1A} = \mathbf{R}_{\mathbf{x}}(\pi/4) \cdot \mathbf{R}_{\mathbf{z}}(\omega) \cdot \mathbf{x} \\
\mathbf{z}_{1B} = \mathbf{R}_{\mathbf{y}}(\pi/4) \cdot \mathbf{R}_{\mathbf{x}}(\omega) \cdot \mathbf{y} \\
\mathbf{z}_{1C} = \mathbf{R}_{\mathbf{z}}(\pi/4) \cdot \mathbf{R}_{\mathbf{y}}(\omega) \cdot \mathbf{z}
\end{cases} \tag{3}$$

Each base axis of the SPM is specifically oriented from one-unit vector of the origin reference frame (\mathbf{x} , \mathbf{y} or \mathbf{z}). The first rotation matrix allows the axis to spin so that of its ω -

inclination is oriented toward the center of the reference frame. The axis \mathbf{z}_{2K} of each arm is then calculated as shown below:

$$\begin{cases}
\mathbf{z}_{2A} = \mathbf{R}_{\mathbf{x}}(\theta_{1A}). \, \mathbf{R}_{\mathbf{z}}(\alpha). \, \mathbf{z}_{1A} \\
\mathbf{z}_{2B} = \mathbf{R}_{\mathbf{y}}(\theta_{1B}). \, \mathbf{R}_{\mathbf{x}}(\alpha). \, \mathbf{z}_{1B}. \\
\mathbf{z}_{2C} = \mathbf{R}_{\mathbf{z}}(\theta_{1C}). \, \mathbf{R}_{\mathbf{y}}(\alpha). \, \mathbf{z}_{1C}
\end{cases} \tag{4}$$

By substituting Eq. (3) and (4) into Eq. (2), the IKM can be developed to obtain a system of equations that involves the input variables θ_{1k} , and the end effector angles (ψ , θ , φ). It is written as followed:

$$\begin{cases} L_{A}\cos(\theta_{1A}) + M_{A}\sin(\theta_{1A}) = N_{A} \\ L_{B}\cos(\theta_{1B}) + M_{B}\sin(\theta_{1B}) = N_{B}, \\ L_{C}\cos(\theta_{1C}) + M_{C}\sin(\theta_{1C}) = N_{C} \end{cases}$$
(5)

With L_k , M_k and N_k , functions of the mechanism geometric parameters α , θ and γ , and the end effector orientation angles ψ , θ and φ . Each of these equation is factorized as followed:

$$\sqrt{L_k^2 + M_k^2} * \left(\frac{L_k}{\sqrt{L_k^2 + M_k^2}} * \cos \theta_{k1} + \frac{M_k}{\sqrt{L_k^2 + M_k^2}} * \sin \theta_{k1} - \frac{N_k}{\sqrt{L_k^2 + M_k^2}}\right) = 0.$$
 (6)

It is then assumed that:

$$\cos \delta = L_k / \sqrt{L_k^2 + M_k^2}$$

$$\sin \delta = M_k / \sqrt{L_k^2 + M_k^2}$$
(7)

Substituting Eq. (7) into Eq. (6) yields to:

$$\cos \delta * \cos \theta_{k1} + \sin \delta * \sin \theta_{k1} = \frac{N_k}{\sqrt{L_k^2 + M_k^2}}.$$
 (8)

The equation above can be solved by isolating the input variables θ_{1k} . For each leg, the input coordinate allowing the end effector to reach the orientation (ψ, θ, φ) is given by the following equation:

$$\theta_{1k} = \cos^{-1}\left(N_k/\sqrt{L_k^2 + M_k^2}\right) + \operatorname{atan2}(M_k, L_k),$$
 (9)

With L_k , M_k and N_k , functions of the mechanism geometric parameters α , θ and γ , the end effector orientation angles ψ , θ and φ and the reconfigurable parameter ω . For each arm of the RSPM, the IKM leads to the same solution as the classical SPM. The difference is that the parametric functions L_k , M_k and N_k now include the variable ω . It can be consequently anticipated that the variable has an impact on the SPM behavior (workspace, kinematic performance, etc.).

3.2. Workspace of the Reconfigurable Spherical Parallel Mechanism

It has been shown in the previous Section that the introduction and variation of the new parameter ω had an impact on the kinematic model of the SPM. Its effect on the workspace and the dexterity are studied. For a given set of geometric parameters, the operational workspace of the Reconfigurable Spherical Parallel Mechanism (RSPM) can be studied by using existence condition of a solution to the inverse kinematic model. By studying Eq. (3), it is found that a set of two conditions per leg should be satisfied:

$$\begin{cases}
L_k^2 + M_k^2 - N_k^2 > 0 \\
L_k^2 + M_k^2 = 1
\end{cases}$$
(10)

For every possible set of orientations (ψ, θ) of the end effector, the conditions given by Eq. (10) is checked for each <u>RRR</u> leg. It is tested in a semi-sphere zone, i.e. $\psi \in [0]$; 360] and $\theta \in [0]$; 90]. The third DoF measured by the angle φ that the SPM provides will

spin the drill around its longitudinal axis. As it is not used here, it will be fixed and the use of this DoF as a reconfigurable parameter will be the subject of further research. In the present study, the spinning angle φ is maintained to 0 as it is intended to study the workspace in Cartesian coordinates. This allows, for a given set of geometric parameters of the SPM, to display its operational workspace as shown on Fig. 9. Preliminary visual observations have revealed a workspace of following characteristics:

- The outside boarder of the workspace has the shape of a spherical equilateral triangle,
 which corners are located near the base of each <u>R</u>RR leg.
- Three circular holes are located near the spherical triangle corners. Their position is symmetrical around the workspace center.

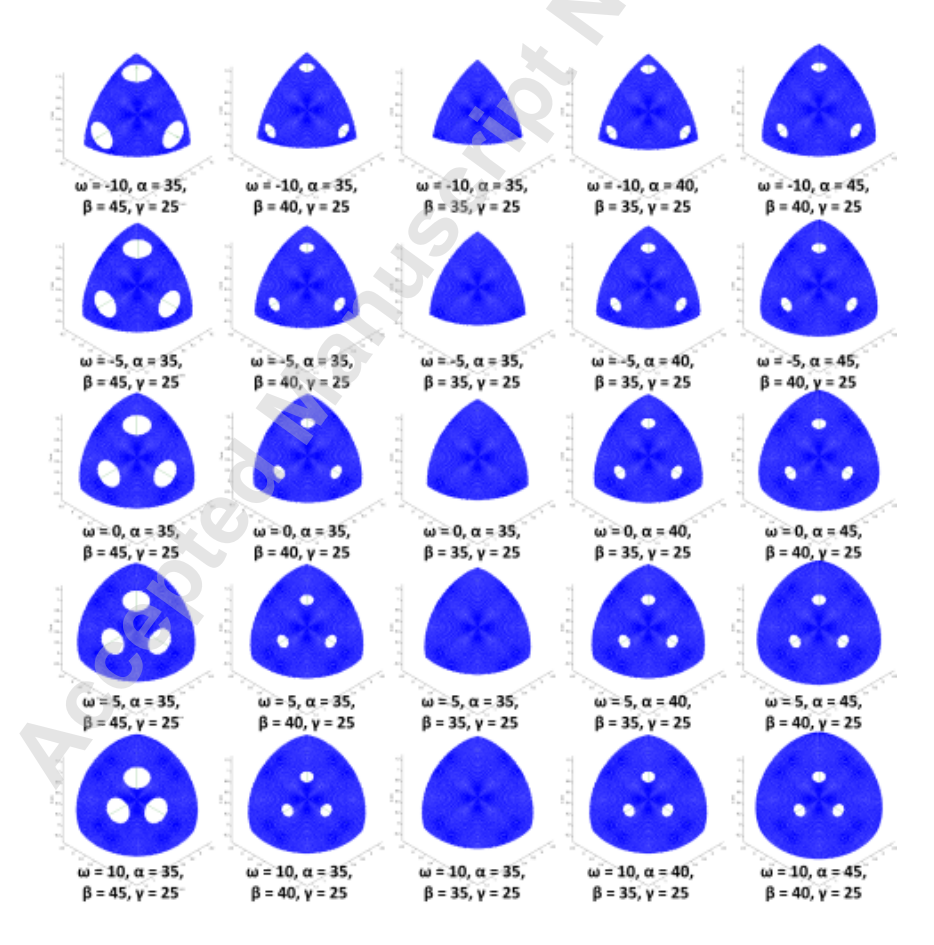


Figure 9. 3-D representation of the 3-RRR RSPM workspace in Cartesian space for several set of geometric parameters (α , β , γ and ω).

Displaying the SPM workspace for several sets of geometric parameters has allowed several observations regarding the effect of these parameters:

- The workspace dimension increases with the sum of parameters α and θ . Therefore, permuting α and θ does not affect the size of the workspace. The location of the hollows does not change (see second and fourth columns of Fig. 9);
- The size of the three holes increases with the difference between α and θ . Therefore, they will disappear when α and θ are equal;
- Increasing the angle γ, which refers to the size of the platform, will increase the dimension of the workspace but will also displace the three holes toward the center.
 For a relatively small value of γ, the holes will cut off the corners of the spherical triangle.

To highlight the influence of the angle ω , the RSPM workspace is displayed for several set of geometric parameters. It can be observed that the geometric parameter ω has a similar effect as γ on the SPM workspace. For a given set of α , θ and γ angles, the outside boarders of the workspace are enlarged while ω is increasing, i.e. when closing the base. Also, the three hollows are progressively moving toward the center of the workspace. On the other hand, opening the base by decreasing ω will reduce the dimension of the outside boarders while the three hollows are moving in toward the workspace corners. If the leg linkage dimensions are small enough and the base "opened" enough, the three hollows partially disappear as they cut off the workspace corners.

The presence of discontinuities in the SPM workspace is a disturbing phenomenon that considerably compromises the manipulator kinematics. This could be avoided by setting the angles α and θ to be equal, or by reducing the size of the platform (angle γ). In order to determine the size and position of these holes, a numerical method is used. The first step consists in locating the boarder of these holes by detecting the change of the result of Eq. (10) over the mechanism workspace. For each hole, the coordinates of their geometric center is calculated by finding the point that minimizes the standard deviation of its distance from all boarder points. When that deviation is extremely low, these distances can be considered as an accurate estimation of the radius between the workspace hole center and its boarder.

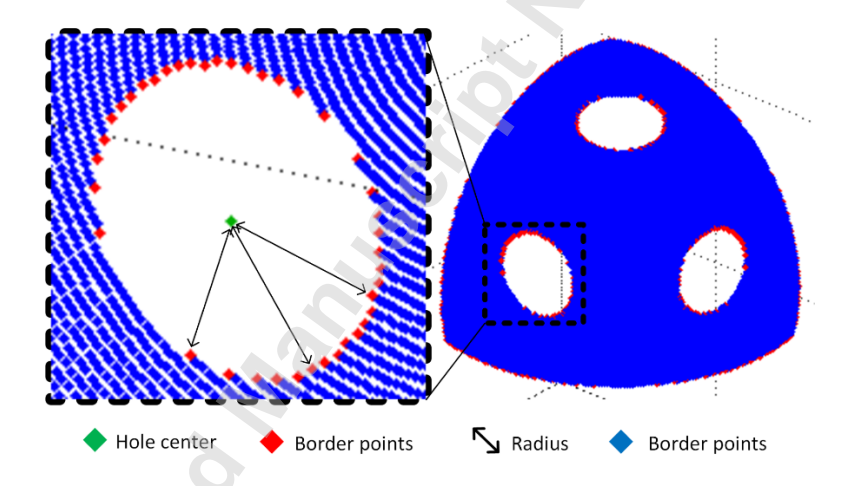


Figure 10. Identification of the workspace holes center.

Based on this method, both the position and the size of the holes can be determined by the coordinate of their center and by their radius, respectively. Also, this method has revealed that these three holes are symmetric. By collecting these data for several set of mechanism parameters, a relationship has been found to determine the size and position of the holes based on the mechanism parameter values. Accordingly to

the preliminary visual observation, the size of the hole depends on the size difference between the proximal and distal linkages of the mechanism leg. Since the hole is located on a spherical surface, its size θ_R is expressed by the angle between its center and its boarder as followed:

$$\sin \theta_R = 0.02 * |\alpha - \beta|. \tag{711}$$

The position of the hole is expressed using angular coordinates. The angle θ_P denotes the angle between the mechanism workspace center axis $\mathbf{z_W}$ and the axis passing by the hole center.

$$\theta_P = \lambda - \gamma - \omega, \tag{12}$$

Where λ , the angle between axes $\mathbf{z}_{\mathbf{W}}$ and \mathbf{x} , \mathbf{y} or \mathbf{z} , as described in Fig. 7.

3.3. Kinematic Performance of the Reconfigurable Spherical Parallel Mechanism

The kinematic performance of the RSPM is computed using the condition number of the mechanism Jacobian matrix **J**. This method is proposed by Gosselin [33] and it can be a reliable measure of dexterity. This index can be written as:

$$\eta = 1/\kappa(\mathbf{J}),\tag{13}$$

Where $\kappa(\mathbf{J}) = \|\mathbf{J}\| \cdot \|\mathbf{J}^{-1}\|$. In the present case, the RSPM Jacobian matrix is obtained by differentiating the IKM given by Eq. (2) with the time. This yields to:

$$\dot{\mathbf{z}}_{2\mathbf{k}}\mathbf{z}_{3\mathbf{k}} + \mathbf{z}_{2\mathbf{k}}\dot{\mathbf{z}}_{3\mathbf{k}} = 0. \tag{14}$$

The velocities of axes $\mathbf{z_{2k}}$ around axes $\mathbf{z_{1k}}$ are given by the velocities of the input variables θ_{1k} and the velocities of axes $\mathbf{z_{3k}}$ around the origin reference frame is given by the angular velocity vector $\boldsymbol{\omega}$. The derivate of axes $\mathbf{z_{2k}}$ and $\mathbf{z_{3k}}$ can then by written as followed:

Journal of Mechanisms and Robotics. Received February 28, 2019; Accepted manuscript posted July 16, 2019. doi:10.1115/1.4044411 Copyright © 2019 basME/Journal of Mechanisms and Robotics

$$\dot{\mathbf{z}}_{2\mathbf{k}} = \dot{\theta}_{1k} \mathbf{z}_{1\mathbf{k}} \times \mathbf{z}_{2\mathbf{k}},\tag{15}$$

$$\dot{\mathbf{z}}_{3\mathbf{k}} = \mathbf{\omega} \times \mathbf{z}_{3\mathbf{k}},\tag{16}$$

With
$$\mathbf{\omega} = \begin{bmatrix} \dot{\theta} \cos(\psi) + \dot{\varphi} \sin(\theta) \sin(\psi) \\ \dot{\theta} \sin(\psi) - \dot{\varphi} \sin(\theta) \cos(\psi) \\ \dot{\psi} + \dot{\varphi} \cos(\theta) \end{bmatrix}$$
.

Equation (15) and (16) are substituted into Eq. (14) to obtain:

$$\mathbf{z}_{1\mathbf{k}} \times \mathbf{z}_{2\mathbf{k}} \cdot \mathbf{z}_{3\mathbf{k}} \dot{\theta}_{1k} = \mathbf{z}_{2\mathbf{k}} \times \mathbf{z}_{3\mathbf{k}} \cdot \boldsymbol{\omega} \tag{17}$$

The mechanism velocity model is then written in a matrix form given by the following equation:

$$\mathbf{B}\dot{\mathbf{q}} = \mathbf{A}\boldsymbol{\omega} \tag{18}$$

With $\dot{\bf q}=\left[\dot{\theta}_{1A}\,\dot{\theta}_{1B}\,\dot{\theta}_{1C}\right]^{\rm T}$ and **A** and **B** the parallel and serial Jacobian matrices, calculated as followed:

$$\mathbf{A} = \begin{bmatrix} (\mathbf{z}_{2\mathbf{A}} \times \mathbf{z}_{3\mathbf{A}})^T \\ (\mathbf{z}_{2\mathbf{B}} \times \mathbf{z}_{3\mathbf{B}})^T \\ (\mathbf{z}_{2\mathbf{C}} \times \mathbf{z}_{3\mathbf{C}})^T \end{bmatrix}, \mathbf{B} = \begin{bmatrix} \mathbf{z}_{1\mathbf{A}} \times \mathbf{z}_{2\mathbf{A}} \cdot \mathbf{z}_{3\mathbf{A}} & 0 & 0 \\ 0 & \mathbf{z}_{1\mathbf{B}} \times \mathbf{z}_{2\mathbf{B}} \cdot \mathbf{z}_{3\mathbf{B}} & 0 \\ 0 & 0 & \mathbf{z}_{1\mathbf{C}} \times \mathbf{z}_{2\mathbf{C}} \cdot \mathbf{z}_{3\mathbf{C}} \end{bmatrix}$$
(19)

Therefore the Jacobian matrix **J** is given by:

$$\mathbf{J} = \mathbf{A}^{-1}.\,\mathbf{B}.\tag{20}$$

As result, the local dexterity of the RSPM is calculated bellow:

$$\eta = 1/\kappa(\mathbf{A}^{-1}.\mathbf{B}). \tag{21}$$

The SPM dexterity distribution is displayed in Fig. 11 for several sets of geometric parameters to highlight the influence of the angle ω . In the present simulations, the graphic display has been adjusted as followed: the variation from orange to red occurs around 0.4 and dark red around 0.6. The yellow is around 0.2. The contrast has been increased to represent the zone outside the workspace in dark blue.

JMR-18-1081, Essomba, 26

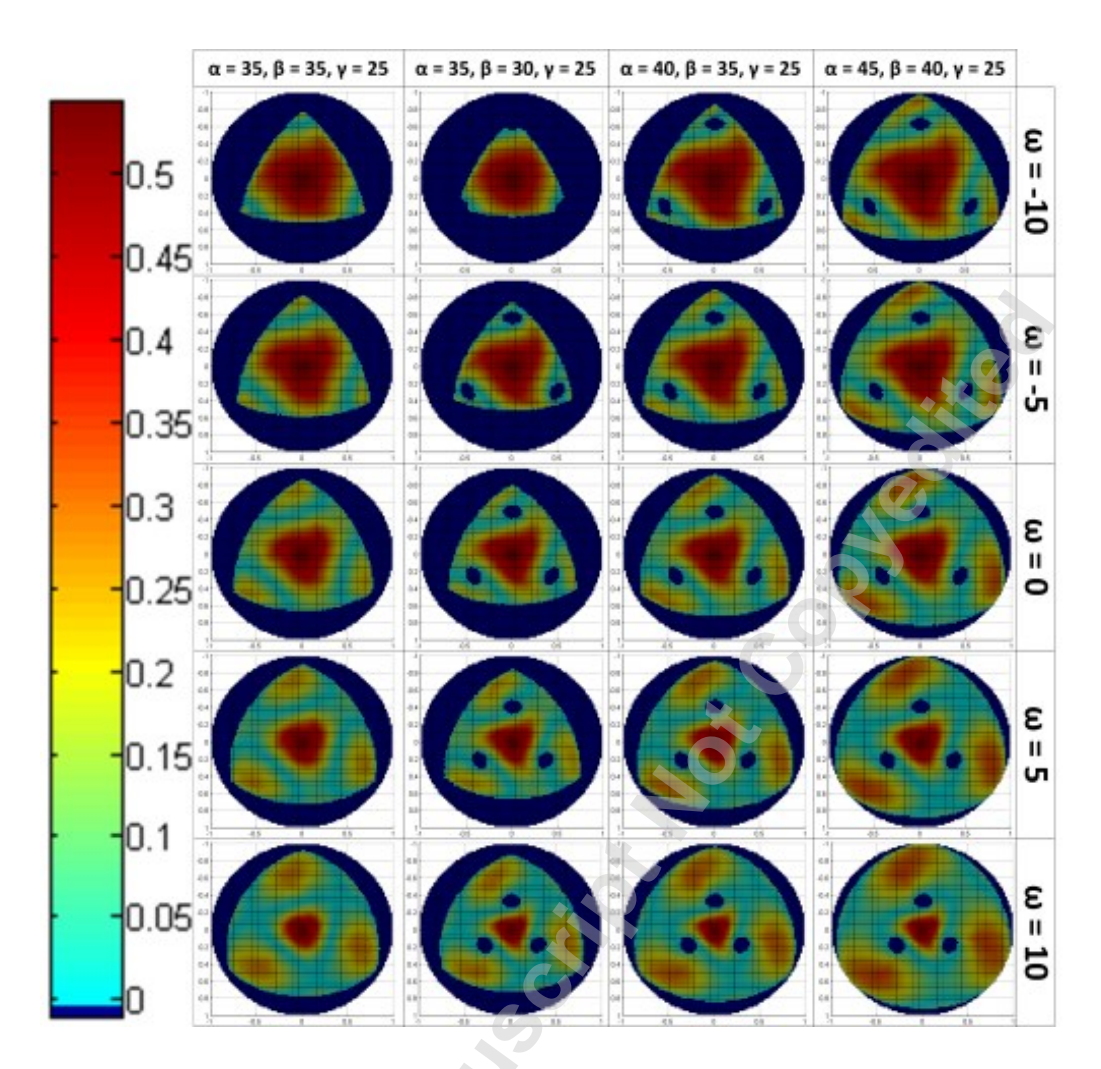


Figure 11. Dexterity distribution of the 3-RRR RSPM for several sets of geometric parameters α , β , γ and ω .

The displacement of the workspace hollows affects the distribution of the mechanism dexterity. Indeed, a lower dexterity can be observed at the proximity of these hollows. As they are moving closer to the workspace center, the zone corresponding to a higher dexterity is reduced, while three new high dexterity zones appear and grow near the workspace corners. This phenomenon is also observed in the absence of workspace hollows when $\alpha=\beta$. Therefore, the distribution of the dexterity over the RSPM over its workspace will present a total of four zone of high local dexterity: one is located at the

center of the workspace, and the three others are disposed before each holes and the workspace boarder. These three satellite zones disappear when the parameter ω is low enough leaving too little space between the holes and the boarder.

The implementation of a new design parameter allows the SPM to generate a new kinematic characteristic in terms of workspace and dexterity. The control of this new parameters while the manipulator end effector is on the move, will permit the adjustment of these characteristics to increase the mechanism performance on a trajectory to its maximum. But the optimization of the RSPM must be first carried out considering the evolution of this parameter.

4. OPTIMIZATION OF THE MECHANISM FOR CRANIOTOMY APPLICATION

An optimization process is proposed to identify the RSPM that generates the highest kinematic performances for the practice of robotic craniotomy. The optimization problem will be formulated and implemented into an algorithm to identify the most suitable mechanism design parameters.

4.1. Optimization Problem Formulation

The optimization method is based on the calculation of a specific index for each mechanism candidate. This index is calculated considering constraint and criteria associated with the practice of craniotomy. So the first step is to identify and to formulate them. The constraint is given by the mechanism operational workspace. Any mechanism candidate validated as a potential solution must be able to cover all the required workspace of the craniotomy identified in Section 2.2. Its end effector must be able to

reach all orientations of the workspace. To evaluate to the check its capacity to cover that workspace, the set of IKM conditions given by Eq. (11) must be verified for the three legs of the RSPM on every possible orientations (ψ , θ). On addition, that same orientation must be reachable over a range of variation of the parameter ω . The two IKM conditions are used for the calculation of two different indexes associated with the optimization constraints. For an orientation of the end effector and ω parameter of the mechanism configuration given by (ψ , θ , ω), two functions C_{k1} and C_{k2} are defined based on Eq. (10) as follow:

$$\begin{cases}
C_{k1}(\psi, \theta, \omega) = L_k^2 + M_k^2 - N_k^2 \\
C_{k2}(\psi, \theta, \omega) = L_k^2 + M_k^2 - 1
\end{cases}$$
(22)

With k = A, B or C. The third function is the defined to indicate if leg of the RSPM can reach an orientation with a given parameter ω .

$$P_k(\psi, \theta, \omega) = \begin{cases} 0 \text{ if } C_{k1} > 0 \text{ and } C_{k2} = 0\\ 1 \text{ otherwise} \end{cases}$$
 (23)

If $P_k(\psi, \theta, \omega) = 0$, the leg k can reach the orientation (ψ, θ) with the parameter ω . If $P_k(\psi, \theta, \omega) = 1$, the leg k cannot reach it. The final function P indicate if the entire RSPM is capable of reaching it and is written as:

$$P(\psi, \theta, \omega) = P_A(\psi, \theta, \omega) + P_B(\psi, \theta, \omega) + P_C(\psi, \theta, \omega). \tag{24}$$

For a given parameter ω , the function P counts the number of leg that cannot reach the orientation (ψ, θ) . It is then integrated into the index $W(\mathbf{I})$ that is calculated as followed:

$$W(\mathbf{I}) = \sum_{\psi=0}^{i} \sum_{\theta=0}^{j} \sum_{\omega=\omega_{min}}^{\omega_{max}} P(\psi, \theta, \omega), \tag{25}$$

With $i=2\pi/\Delta\psi$ and $j=\theta_{max}/\Delta\theta$. The variables $\Delta\psi$ and $\Delta\theta$ will be used to adjust the algorithm resolution, i.e. the distance between two successive point of the RSPM to calculate the index $W(\mathbf{I})$. This index indicate for a given mechanism $\mathbf{I}=[\alpha \beta \gamma]$, the number of instances where a leg was unable to reach an orientation. When $W(\mathbf{I})=0$, the mechanism \mathbf{I} is capable of reaching all orientations of the workspace for a parameter ω from ω_{min} to ω_{max} .

While the optimum RSPM for craniotomy must satisfy the workspace constraint, it must generate the highest dexterity over its workspace and for a certain range of variation on the parameter ω . For an orientation (ψ,θ) with the parameter ω , the local dexterity is calculated as presented in Section 3.3: using the conditioning number of the Jacobian matrix as established by Eq. (21). On a single orientation (ψ,θ) , the conditioning number is calculated for several values of ω and its highest value is collected. The local dexterity can be written as:

$$\eta(\psi, \theta) = \max_{\omega} (1 - (1/\kappa(\mathbf{J}))), \tag{26}$$

With $\omega \in [\omega_{min}; \omega_{max}]$. The value of the local dexterity has been adjusted to make it compatible with the use of an optimization process that usually search to minimize an index. As it is defined here, its range of values will be comprised between 0 and 1 and a low value will correspond to a high dexterity. All the local dexterities are then used to calculate the average dexterity over the workspace, which is the index used for the optimization. The criterion $K(\mathbf{I})$ is calculated as followed:

$$K(\mathbf{I}) = \sum_{\psi=0}^{i} \sum_{\theta=0}^{j} \eta(\psi, \theta). \tag{27}$$

Considering the constraint and the criterion defined above, the entire optimization process can be formulated as bellow:

$$\begin{cases}
Minimize(K(\mathbf{I})) \\
Subjet to W(\mathbf{I}) = 0 \\
\mathbf{I} = [\alpha \quad \beta \quad \gamma] \\
x_i \in \mathbf{I}, \ x_i \in [x_{i_{min}}; x_{i_{max}}]
\end{cases}$$
(28)

Where $K(\mathbf{I})$ and $W(\mathbf{I})$ are respectively given by Eqs. (27) and (25). This formulation has to be implemented in an optimization algorithm using a specific method.

4.2. Optimization Method and Results

To identity the optimum 3-RRR RSPM for craniotomy, a Genetic Algorithm is used to manipulate a population of several mechanism individuals represented by their characteristics (their design variables) over several generations. Based on these evolving characteristics, these individuals will be filtered through the optimization constraint given by W(I), evaluated through the optimization criterion given by K(I) and ranked by the algorithm to select only the best individuals. The best individuals are then preserved and transferred into the next generation, while the other individuals are eliminated as they are seen as weakest. The GA will then repopulate the next generation by creating new individuals through crossover and mutation process. The crossover process will randomly combine the characteristics of two "parent" individuals to generate a new "child" individual. Then, the mutation process will randomly modify some characteristic of some individuals. Therefore, the linkage dimensions of a population of 3-RRR RSPM will be manipulated similarly as genetic characteristics. As the number of generations increases, the individuals of the population shall convert to one or several optimum individual

models. When the deviation of their respective performance in terms of dexterity is below the termination criterion (10^{-6} in the present case), the current generation is considered as optimum and an individual can be selected out of this population. One of these optimal individual will be selected as the final 3-RRR RSPM for craniotomy.

A fitness function has been programmed on Matlab to determine the performance of one mechanism at a time. The input data of this function is the design vector that represents one mechanism individual and containing its design variables. The output value of this function is the value of the index $K(\mathbf{I})$. The constraint given by the index $W(\mathbf{I})$ is checked in the same function. For each possible orientation (ψ, θ) of the required workspace, the corresponding input variables θ_{AI} , θ_{BI} and θ_{CI} are calculated for several parameter ω between ω_{min} and ω_{max} . Based on these values, the dexterity is then calculated and the maximum value is saved. For each orientation, the algorithm will collect the maximum dexterity value over a range of ω and the average of these maximum values is used to calculate the mechanism global dexterity, which is given by $K(\mathbf{I})$. As the input variables are calculated, the function will interrupt as soon as a complex value is found, i.e. if $Im(\theta_{KI}) \neq 0$. It will then return a penalty value of $K(\mathbf{I})$ to insure that the individual will be eliminated from the next generation.

The available Matlab software has an integrated GA function that was used in the present optimization by calling the fitness function. Its parameters have been adjusted to manipulate a population of 100 individuals over 200 generations. The individual characteristics are defined within the following ranges:

$$\alpha \in [30; 45] \quad \beta \in [30; 45] \quad \gamma \in [20; 30]$$
 (29)

JMR-18-1081, Essomba, 32

Each RSPM of a generation is evaluated by the fitness function described above based on its characteristics. As stated in Section 2.2, the workspace required for craniotomy has a maximum angle θ_{max} of 20 degrees. Also, the range of value on the parameter ω is [-10; 10]. These values have been used in the fitness function. The GA has been run with all parameters mentioned above and has identified at the 54th generation the optimum individual with the following characteristics:

$$I_{opt} = [41 \ 41 \ 30]$$
 (30)

The optimum 3- \underline{R} RR RSPM I_{opt} can cover all the required workspace and has a global dexterity of 0.53, when considering the dexterity given by Eq. (21), i.e. the higher the better. The distribution of its local dexterity is displayed on Fig. 12-(a). It from 0.46 to 0.79, when the parameter ω is allowed to vary from -10 to 10 degrees.

The dimensions identified by Eq. (30) are considered to be the optimum ones for the 3-RRR RSPM to perform a craniotomy, but the optimization process used only allow to compare one type of architecture at a time. The mechanism I_{opt} shall be therefore compared with other type of SPM.

5. EVALUATION AND SIMULATIONS ON THE OPTIMUM MECHANISM

The optimum mechanism identified in the previous Section is evaluated. Its ability to generate a high dexterity on craniotomy trajectories is investigated.

5.1. Behavior of the RSPM base reconfigurable parameter

The variation of the parameter ω that generates the maximum dexterity is studied to insure that it will be possible to control it in a future mechanism prototype. The

evolution of this parameter over the RSPM workspace is calculated and displayed on Fig. 12. It shows that the evolution of this parameter does not suffer from any discontinuity, proving that the angle ω could be controlled smoothly in an active prototype. Also, the angle ω goes from -10 to 9 degrees which represents almost all the range of variation allowed by the algorithm. The base reconfiguration parameter increases when the end effector is moving toward the mechanism workspace center. And it decreases when the end effector the moving away from the center. Therefore, the RSPM can maintain higher kinematic performance by "closing" its reconfigurable base as it is operating near the workspace center and by "opening" it as it is working away from the center. Although it seems that the range of the angle ω could be increased to generate a better dexterity, the range fixed in Section 4.2 appears to be a reasonable limit according to our preliminary studies. Indeed, below -10 degrees, the mechanism workspace is often compromised as each RRR leg is too far from point to reach. This problem could be solved by increasing the size of the mechanism legs, which is what the GA did in this case. But on the hand, excessive linkage lengths would result other issues such as possible collisions. Above 10 degrees, the first joint of the mechanism legs are too close from the workspace, which decrease its global dexterity as the singular configuration are approaching the workspace.

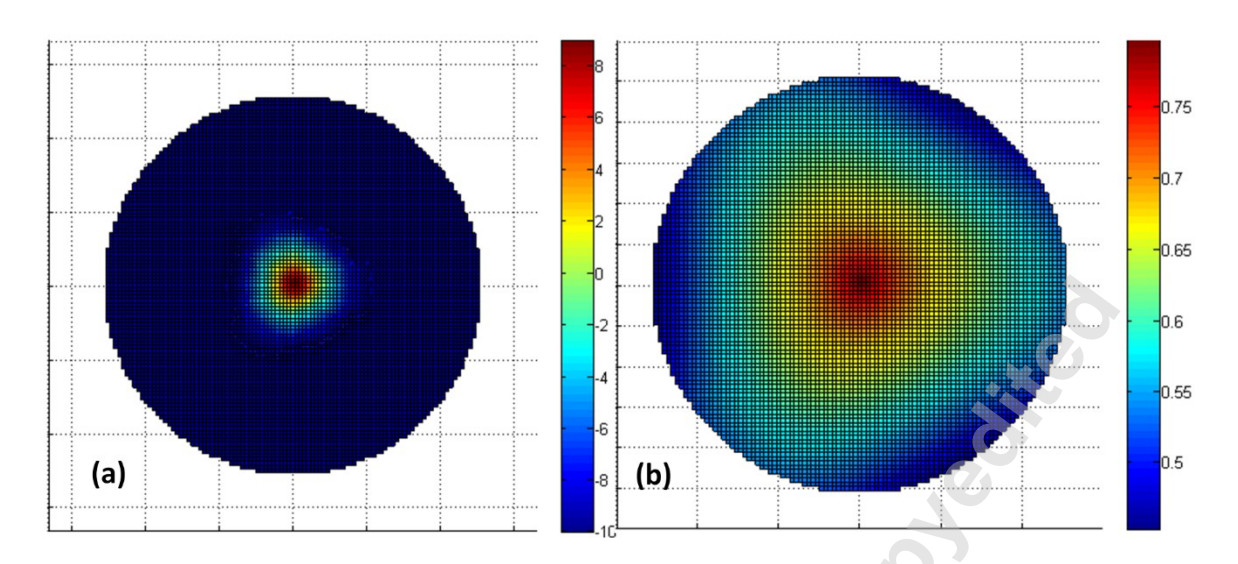


Figure 12. (a) Variation of the parameter ω for maximum dexterity over the craniotomy workspace. (b) Distribution of the resulting local dexterity over the craniotomy workspace.

The behavior of the parameter ω is now evaluated on the trajectories identified during the motion capture experiments on Human cadavers in Section 2.2. Each point of these trajectories corresponds to an orientation of the surgical drill given by the Euler angles (ψ, θ) . An algorithm has been programmed to calculate, for each orientation of these trajectories, the parameter ω that generates the highest dexterity. The evolution of the parameter ω on these trajectories are all displayed on Fig. 13. This study reveals that this evolution of the angle ω on trajectories for craniotomy appears to be controllable as no discontinuity can be observed.

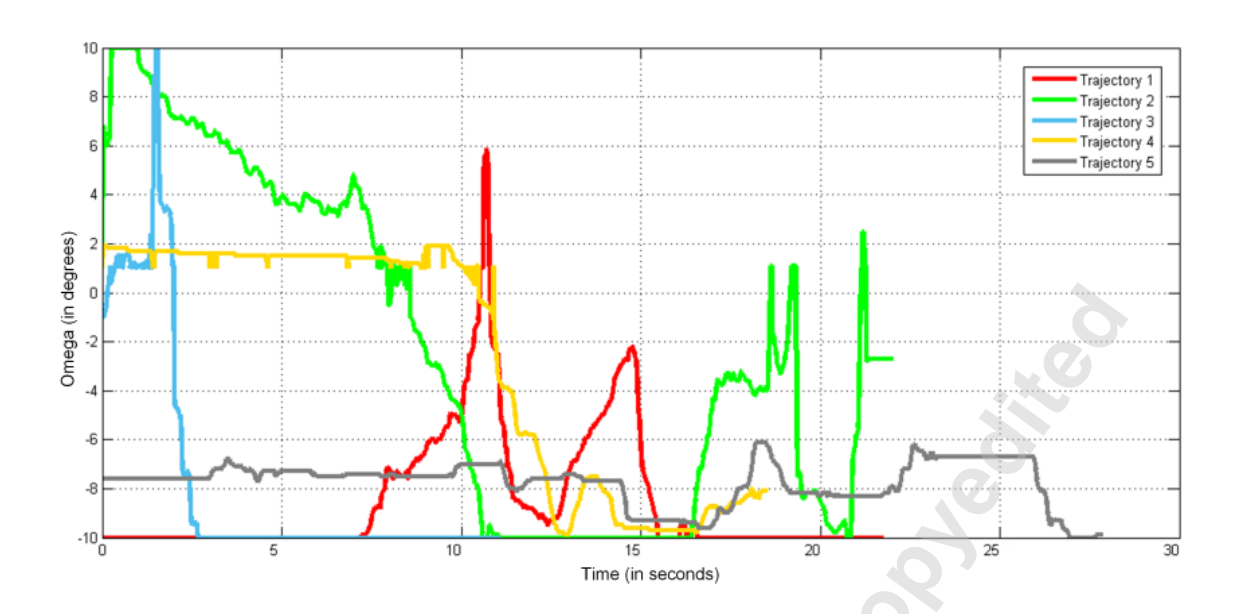


Figure 13. Evolution of the parameter ω generating the maximum dexterity on craniotomy trajectories.

5.2. Comparison with classical SPM

The contribution of its base configuration using the parameter ω is studied. In order to demonstrate the contribution of the architectural improvement on RSPM, it is now compared to the classical 3-RRR SPM with a trihedral base as seen in Fig. 6. The active revolute joint axes of each leg are orthogonal and not adjustable. It is referred to as Trihedral Spherical Parallel Mechanism (TSPM). No example of such mechanisms optimized for craniotomy in terms of dexterity over the same workspace can be found in the literature. Consequently, the TSPM have been identified through a similar optimization process as the one presented in Section 4.1. Therefore, the TSPM for craniotomy is identified though a GA as well. The GA parameters are modified to manage a population of TSPM that has the same design variables and research range as the RSPM as described in Eq. (29). The difference is that the parameter ω in the fitness function is fixed to zero, which corresponds to a trihedral configuration of the base. So the local

JMR-18-1081, Essomba, 36

dexterity will be calculated for an orientation (ψ, θ) with $\omega = 0$ and there will be no need to select the highest value. The GA algorithm has been run and has resulted an optimum TSPM with the following design variables:

$$I_{TSPM} = [41 \ 41 \ 30]$$
 (31)

The TSPM design variables are the same as the RSPM. The evolution of their respective local dexterity are tested on the same craniotomy trajectories identified in Section 2.2. An algorithm has been programmed to calculate, for each orientation of these trajectories, the local dexterity of the TSPM. For the RSPM, the local dexterity will depend on the parameter ω . So for each point of the trajectories, the highest local dexterity will be considered for comparison with the TSPM. The evolution of the dexterity on one trajectory is given as an example of trajectory in Fig. 14. It shows that the RSPM has a dexterity always higher than the TSPM on this trajectory. The difference between the RSPM and the TSPM dexterity has an average of +2.23% with a maximum of +13.6%. This illustration shows that the RSPM can reconfigure on a trajectory to maintain a higher dexterity than the classical SPM.

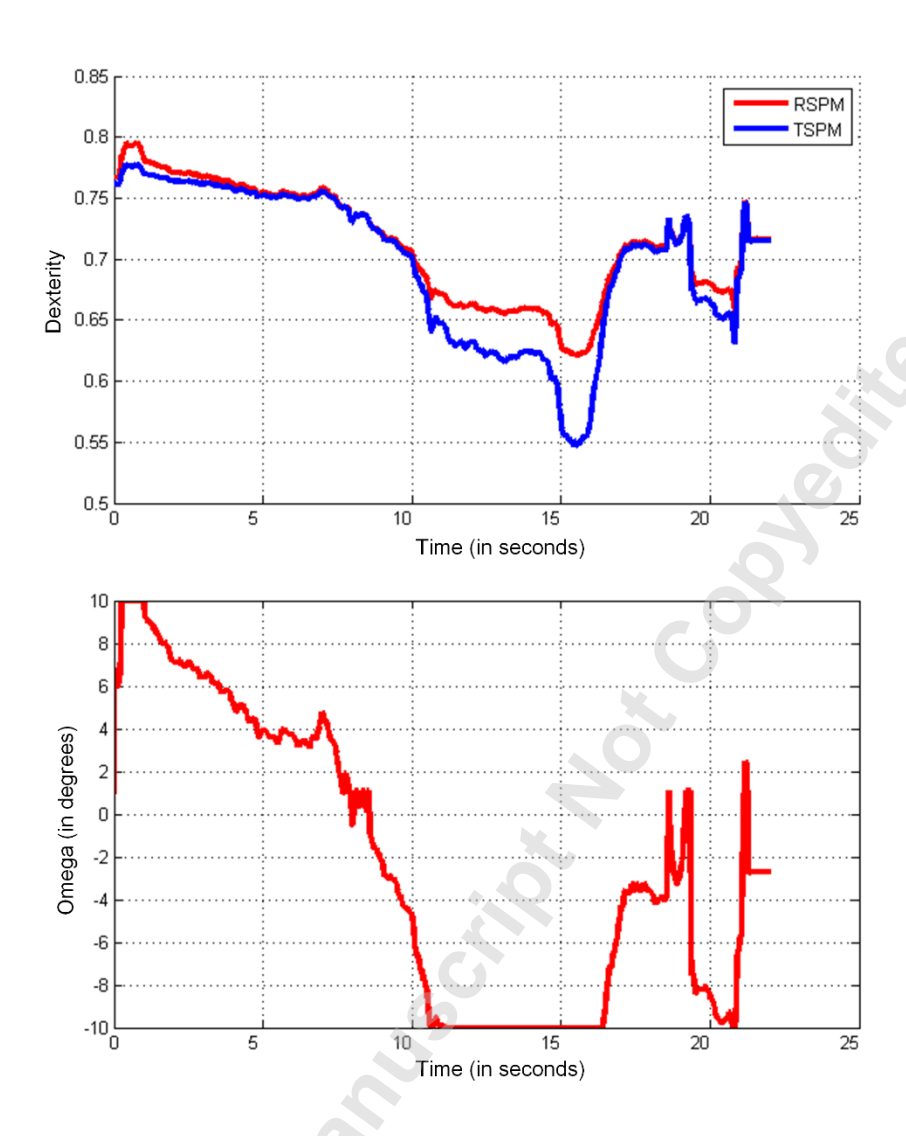


Figure 14. Evolution of the RSPM and TSPM dexterities on a craniotomy trajectory and evolution of the RSPM corresponding reconfigurable parameter.

For all craniotomy trajectories, the difference between the RSPM and TSPM dexterities is considered to evaluate the improvement of the RSPM. The improvement in calculated and displayed on Fig. 15.

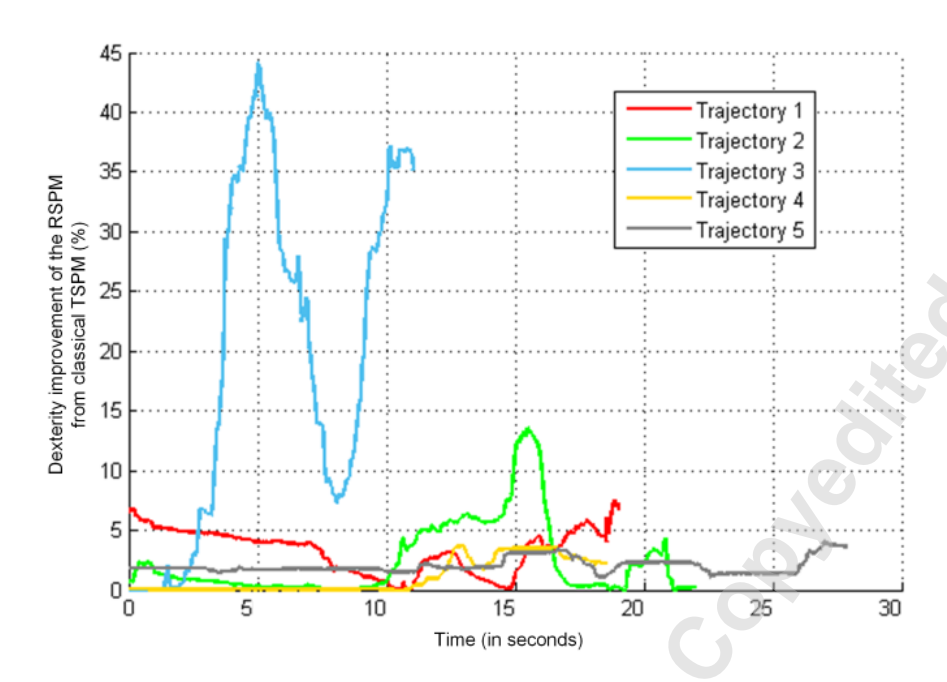


Figure 15. Difference between the RSPM and TSPM dexterities over the craniotomy trajectories.

On average, the RSPM is capable of generating a dexterity 5.5% higher than the TSPM on all the trajectories measured for craniotomy. The maximum local dexterity improvement on a trajectory has been calculated to 44.3%. The numerical results obtained from these simulations are all presented in Table 2.

Table 2. Comparison between the RSPM and TSPM dexterities.

Trainatam	Mechanism	<u>O</u>	Dexterity	Dexterity improvement			
Trajectory		Minimum	Average	Maximum	Average	Maximum	
1	TSPM	0.603	0.678	0.760	3.29%	7.55%	
	RSPM	0.648	0.657	0.765	3.29%		
2	TSPM	0.547	0.697	0.796	2.23%	13.59%	
	RSPM	0.621	0.713	0.777	2.23%		
3	TSPM	0.388	0.540	0.775	18.84%	44.3%	
	RSPM	0.555	0.625	0.791	10.04%		
4	TSPM	0.649	0.711	0.745	1.07%	3.69%	
4	RSPM	0.673	0.718	0.645	1.07/0		
5	TSPM	0.645	0.673	0.690	2.02%	4.05%	
	RSPM 0.67	0.671	0.687	0.697	2.02/0	4.03/0	

Although the difference between the maximum dexterity reached by the RSPM and by the TSPM appears to be very limited, the difference between both mechanisms minimum dexterity is much larger. On the one hand, the RSPM has maximum dexterity only 0.13 to 2.44% higher the TSPM, on the other hand, it has a minimum dexterity 3.70 to 43.04% higher. It seems that the major contribution of the base reconfiguration parameter is to prevent significant decrease of dexterity while the SPM is moving its end effector away from the workspace center zone. This tendency can be observed in the Fig. 14. Therefore, the RSPM behavior appears to be more stable than the TSPM in terms of kinematic performances.

6. CONCLUSION

In the present work, a mechanism has been proposed to perform craniotomy. The base configuration of a 3-RRR SPM has been studied in order to introduce a new parameter that can be used as to reconfiguration variable. The mechanical method to control its value consists in using three pantographic linkages. The influence of this parameter on the mechanism workspace and dexterity distribution has been investigated. It has permitted a series of promising observations and a numerical analysis has allowed determining relationships between the base configuration variable and the workspace geometric characteristics. A series of motion capture experiments have allowed to measure the motion of a surgical drill during craniotomy on Human cadavers. The data collected have allowed the kinematic optimization of the proposed RSPM. The kinematic performance optimum mechanism has been tested on the craniotomy

JMR-18-1081, Essomba, 40

trajectories issued from the motion capture experiments. The results showed that the RSPM generates higher and more stable dexterity than the classical SPM. This represents an improvement in terms of safety would this mechanism be used for a robotic assisted craniotomy.

ACKNOWLEDGMENT

The experimentations presented in Section 2.1 have been carried out thanks to the Anatomy and Biomechanical Simulation Lab. of the College of Medicine and Pharmacy of the University of Poitiers. Also, we would like to express our deepest gratitude to the people who donated their body for medical research.

FUNDING

This study has been financially supported by a research collaboration project between French CNRS and Taiwanese MOST, under grant No. PRC2142 (CNRS) and 107-2911-I-008-505 (MOST).

REFERENCES

- [1] Bast, P., Popovic, A., Wu, T., Heger, S., Engelhardt, M., Lauer, W., Radermacher, K., Schmieder, K., "Robot-and computer-assisted craniotomy: resection planning, implant modelling and robot safety," International Journal of Medical Robotics and Computer Assisted Surgery, 2006, 2, pp. 168-178.
- [2] Hsiao, M.-H., Kuo, C.-H., 2012, "A Review to the Powered Drilling Devices for Craniotomy," Journal of Medical Devices, 6(1), pp. 017557.
- [3] Bofinger, G., Wolfle, W., 1982, "Skull Trepanation Drill," U.S. Patent No. 4,319,577, Washington, DC: U.S. Patent and Trademark Office.
- [4] Ahola, J. J., Harris, D. G., 1999, "Blade Guard for a Surgical Tool," U.S. Patent No. 6,001,115, Washington, DC: U.S. Patent and Trademark Office.
- [5] Burghart, C., Raczkowsky, J., Rembold, U., Wörn, H., 1998, "Robot Cell for Craniofacial Surgery," Proceedings of the 24th Annual Conference of the IEEE Industrial Electronics Society, Aachen, Germany, 31 August-4 September, pp. 2506-2511.
- [6] Sim, C., Ng, W. S., Teo, M. Y., Loh, Y. C., Yeo, T. T., 2001, "Image-Guided Manipulator Compliant Surgical Planning Methodology for Robotic Skull-Base Surgery," International Workshop on Medical Imaging and Augmented Reality, Shatin, Hong Kong, China, 10-12 June, pp. 26-29.
- [7] Federspil, P. A., Geisthoff, U. W., Henrich, D., Plinkert, P. K., 2003, "Development of the First Force-Controlled Robot for Otoneurosurgery," Laryngoscope, 113(3), pp. 465-471.
- [8] Korb, W., Engel, D., Boesecke, R., Eggers, G., Kotrikova, B., Marmulla, R., Raczkowsky, J., Wörn, H., Mühling, J., Hassfeld, S., 2003, "Development and First Patient Trial of a Surgical Robot for Complex Trajectory Milling," Computer Aided Surgery, 8(5), pp. 247-256.
- [9] Weimin, S., Jason, G., Yanjun, S., 2006, "Using Tele-Robotic Skull Drill for Neurosurgical Applications," Proceedings of the IEEE International Conference on Mechatronics and Automation, Luoyang, China, 25-28 June, pp. 334-338.
- [10] Tsai, T. C., Hsu, Y. L., 2007, "Development of a Parallel Surgical Robot with Automatic Bone Drilling Carriage for Stereotactic Neurosurgery," Biomedical Engineering: Applications, Basis and Communications, 19(4), pp. 269-277.
- [11] Matinfar, M., Baird, C., Batouli, A., Clatterbuck, R., Kazanzides, P., 2007, "Robot-Assisted Skull Base Surgery," Proceedings of the IEEE/RSJ International Conference on Intelligent Robots and Systems, San Diego, CA, USA, 29 October-2 November, pp. 865-870.
- [12] Cunha-Cruz, V., Follmann, A., Popovic, A., Bast, P., Wu, T., Heger, S., Engelhardt, M., Schmieder, K., Radermacher, K., 2010, "Robot- and computer-assisted craniotomy (CRANIO): from active systems to synergistic man-machine interaction," Proceedings of the Institution of Mechanical Engineers, Part H: Journal of Engineering in Medicine, 224(3), pp. 441-452.
- [13] Kobler, J. P., Kotlarski, J., Öltjen, J., Baron, S., Ortmaier, T., 2012, "Design and Analysis of a Head-Mounted Parallel Kinematic Device for Skull Surgery," International Journal of Computer Assisted Radiology Surgery, 7(1), pp. 137-149.

- [14] Li, G.-K., Essomba, T., Wu, C.-T., Lee, S-T., 2016, "Kinematic design and optimization of a novel dual-orthogonal remote center-of-motion mechanism for craniotomy," Proceedings of the Institution of Mechanical Engineers, Part C: Journal of Mechanical Engineering Science, 231(6), pp. 1129-1145.
- [15] Essomba T., Wu, C.-T., Lee, S.-T., Kuo, C.-H., 2016, "Mechanical Design of a Craniotomy Robotic Manipulator Based on Optimal Kinematic and Force Performance," Robotics and Mechatronics, Mechanisms and Machine Science series, 37, pp. 191-198.
- [16] Dehghani, M., Moghadam, M.M., Torabi, P., 2018, "Analysis, optimization and prototyping of a parallel RCM mechanism of a surgical robot for craniotomy surgery", Industrial Robot: An International Journal, 45(1), pp. 78-88.
- [17] Essomba, T., Laribi, M.A., Hsu, Y., Zeghloul, S., 2018, "Kinematic Analysis of a 3-RRR Spherical Parallel Mechanism with Configurable Base," Proc. of the 4th IFToMM *Symposium on Mechanism Design for Robotics*, A. Gasparetto et al., eds., Springer, Cham, Udine, Italy, pp. 101-109.
- [18] Gosselin, C. M., Lavoie, E., 1993, "On the kinematic design of spherical three-degree-of-freedom parallel manipulators," The International Journal of Robotics Research, 12(4), pp. 393-402.
- [19] Gosselin, C. M., St-Pierre, E., Gagne, M., 1996, "On the development of the agile eye: mechanical design, control issues and experimentation," IEEE Robotics and Automation Society Magazine, 3(4), pp. 29-37.
- [20] Cammarata, A., Sinatra, R., 2008, "The elastodynamics of the 3-CRU spherical robot," Second International Workshop on Fundamental Issues and Future Directions for Parallel Mechanisms and Manipulators, N. Andreff, O. Company, M. Gouttefarde, S. Krut, F. Pierrot, editors, pp. 159-165.
- [21] Li, R., Guo, Y., 2014, "Research on dynamics and simulation of 3-RRP spherical parallel mechanism," Third International Workshop on Fundamental Issues and Future Directions for Parallel Mechanisms and Manipulators, pp. 7-8.
- [22] Huda, S., Takeda, Y., Hanagasaki, S., 2008, "Kinematic design of 3-URU pure rotational parallel mechanism to perform precise motion within a large workspace," Second International Workshop on Fundamental Issues and Future Directions for Parallel Mechanisms and Manipulators, N. Andreff, O. Company, M. Gouttefarde, S. Krut, F. Pierrot, editors, pp. 49-56.
- [23] Herve, J. M., Karouia, M., 2002. "The novel 3-RUU wrist with no idle pair," First International Workshop on Fundamental Issues and Future Directions for Parallel Mechanisms and Manipulators, C. M. Gosselin, I. Ebert-Uphoff editors, pp. 284-286.
- [24] Essomba, T., Laribi, M.A., Gazeau, J.P., Poisson, G., Zeghloul, S., 2012, "Contribution to the design of a robotized tele-echography system," Frontiers of Mechanical Engineering, Special Issue on International Symposium on Robotics and Mechatronics, Vol. 7(2), pp. 135-149.
- [25] Essomba, T., Laribi, M.A., Zeghloul, S. Poisson, G., 2016, "Optimal synthesis of a spherical parallel mechanism for medical application," Robotica, Vol. 34(3), pp. 671-688. [26] Luces, M., Mills, J. K., Benhabib, B., 2017, "A review of redundant parallel kinematic mechanisms," Journal of Intelligent & Robotic Systems 86(2), pp. 175-198.

- [27] Yim M., Zhang, Y., Duff, D., 2002, "Modular robots," Feature article, IEEE Spectrum, 39(2), p. 30-34.
- [28] Zhang, X., Zhang, X., 2016, "A comparative study of planar 3-RRR and 4-RRR mechanisms with joint clearances," Robotics and Computer-Integrated Manufacturing, **40**, pp. 24-33.
- [29] Azulay, H., Mahmoodi, M., Zhao, R., Mills, J.K., Benhabib, B., 2014, "Comparative analysis of a new 3-PPRS parallel kinematic mechanism," Robotics and Computer-Integrated Manufacturing, **30**, pp. 369-378.
- [30] Gan, D., Dai, J.S., Sanevirane, L., 2013, "Reconfigurability and unified kinematics modeling of a 3rTPS metamorphic parallel mechanism with perpendicular constraint screws," Robotics and Computer-Integrated Manufacturing, **29**, pp. 131-128.
- [31] Huang, G., Guo, S., Zhang, D., Qu, H., Tang, H., 2018, "Kinematic analysis and multi-objective optimization of a new reconfigurable parallel mechanism with high stiffness," Robotica, **36**(2), pp. 187-203.
- [32] Kang, X., Dai, J. S., 2019, "Relevance and Transferability for Parallel Mechanisms with Reconfigurable Platforms," Journal of Mechanisms and Robotics, **11**(3), 031012.
- [33] Gosselin, C., Angeles, J., 1991, "A global performance index for the kinematic optimisation of robotic manipulators," ASME Journal of Mechanical Design, **113**(3), pp. 220–226.

Table Caption List

Table 1 Bounding values for orientation angles.

Table 2 Comparison between the RSPM and TSPM dexterities.

Figure Captions List

- Fig. 1 "Rosen burr" type surgical drill for craniotomy.
- Fig. 2 Left: Scheme of the used Qualisys motion capture system, including 8

 Miqus cameras, a camera cable, a power unit, and a computer. Right:

 Reflective markers on surgical drill and cadaver's skull.
- Fig. 3 Anatomical zones of interest for the neurosurgeon.
- Fig. 4 Kinematic of the surgical drill in craniotomy.
- Fig. 5 Range of orientation angles for all locations on the skull.
- Fig. 6 Kinematic drawing of the 3-RRR Spherical Parallel Mechanism.
- Fig. 7 Kinematic of the base SPM reconfigurable base.
- Fig. 8 Conceptual CAD of the 3-RRR Reconfigurable Spherical Parallel Mechanism.
- Fig. 9 3-D representation of the 3-RRR RSPM workspace in Cartesian space for several set of geometric parameters (α , β , γ and ω).
- Fig. 10 Identification of the workspace holes center.
- Fig. 11 Dexterity distribution of the 3-RRR RSPM for several sets of geometric parameters α , β , γ and ω .
- Fig. 12 Variation of the parameter ω for maximum dexterity over the craniotomy workspace. (b) Distribution of the resulting local dexterity over the craniotomy workspace.

Fig. 13	Evolution	of the	parameter	ω	generating	the	maximum	dexterity	on
	craniotom	y trajed	ctories.						

- Fig. 14 Evolution of the RSPM and TSPM dexterities on a craniotomy trajectory and evolution of the RSPM corresponding reconfigurable parameter.
- Fig. 15 Difference between the RSPM and TSPM dexterities over the craniotomy trajectories.